

Electronic Supplementary Information

Siloxene nanosheet: A metal-free semiconductor for water splitting

Shuang Li,^a Hui Wang,^a Dandan Li,^b Xiaodong Zhang,^{*a} Yufeng Wang,^a Junfeng Xie,^a Jingyao Wang,^a Yupeng Tian,^b Wenxiu Ni^c and Yi Xie^{*a}

^a Hefei National Laboratory for Physical Sciences at the Microscale, Collaborative Innovation Center of Chemistry for Energy Materials, University of Science and Technology of China, Hefei, Anhui, 230026, P. R. China

^b Department of Chemistry, Anhui University, Hefei, Anhui, 230039, P. R. China

^c Department of Chemistry, Shantou University, Shantou, 515063, P. R. China

S1. Experimental section

Preparation of ultrathin siloxene nanosheets: According to previous reports, different configurations of siloxene can be prepared from a reaction of CaSi_2 power with different methods.¹⁻⁴ In this work, the ultrathin siloxene nanosheets were prepared using a modified method proposed by Weiss et al.¹ In a typical synthesis, approximately 0.8 g of CaSi_2 was immersed in 100 mL of 37% HCl at 0 °C. The mixture was stirred continuously for 3 days under Ar atmosphere. The resulting yellow-green solid power was collected by centrifuging the mixture, washed with acetone for many times to remove the hydrochloric acid solution and then dried at 60 °C under vacuum. Of note, the obtained products need further purification before used for characterization to remove a small amount of unreacted CaSi_2 nanoparticles and large-area siloxene nanosheets.

Characterization: The transmission electron microscopy (TEM) image was carried out on a JEM-2100F field emission electron microscope at an acceleration voltage of 200 kV. High-angle annular dark-field scanning transmission spectroscopy (HAADF-STEM) image and corresponding energy-dispersive spectroscopy (EDS) mapping analyses were performed on a JEOL JEM-ARF 200F TEM/STEM with a

spherical aberration corrector. Atomic force microscopy (AFM) measurement was performed by means of Veeco DI Nanoscope Multi Mode V system. The field emission scanning electron microscopy (FE-SEM) images were taken on a JEOL JSM-6700F SEM. X-ray photoelectron spectra (XPS) was acquired on an ESCALAB MK II with Mg K_{α} as the excitation source. X-ray absorption near-edge structure (XANES) measurements were conducted on the X-ray Magnetic Circular Dichroism End-station at Hefei Synchrotron Radiation Facility in the University of Science of Technology of China. Raman spectra was recorded at room temperature with a LABRAM-HR Confocal Laser Micro Raman Spectrometer 750 K with a laser power of 0.5 mw. The Fourier transform infrared (FT-IR) spectra were measured on a Magna-IR 750 FT-IR spectrometer in a KBr pellet, scanning from 4000 to 400 cm^{-1} at room temperature. The UV-vis absorption spectrum was recorded on a Perkin Elmer Lambda 950 UV-vis-NIR spectrophotometer. The photoluminescence (PL) spectrum was obtained by using a FLUOROLOG-3-TAU fluorescence spectrometer equipped integrating sphere. Electron spin resonance (ESR) measurements were performed using a Bruker EMX plus model spectrometer operating at X-band frequencies (9.4 GHz) at room temperature.

Calculation details: The optimization was done by B3LYP (6-31 G(d)) with Cs symmetry constraints. Then, TDDFT calculations were performed on the optimized structure. All the calculations including optimization and TDDFT were conducted in G03 software. Geometry optimization and TDDFT calculation were calculated with a basis set composed by 6-31G for silicon, hydrogen and oxygen atoms.

Photocatalytic test: Photocatalytic water splitting reactions were carried out in a Pyrex top-irradiation reaction vessel connected to a closed glass gas system. The reaction vessel was soaked in an outer vessel in which cooling water circulated to keep the temperature of the reaction solution at room temperature. In detail, 50 mg powdered siloxene nanosheets were dispersed in 200 mL of pure water by sonication. The obtained reactant dispersion was put into the reaction vessel and stirred. The reaction system was evacuated several times to remove air completely prior to irradiation under a 300 W Xe lamp , full spectrum irradiation, 150 mW/cm^2 . The

evolved gases were analyzed by gas chromatography.

Total H₂O₂ (including bounded ones and H₂O₂ in solution) test with *o*-tolidine:

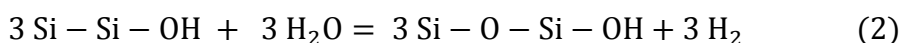
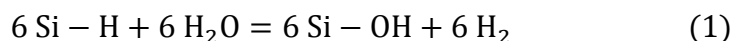
Hydrogen peroxide (H₂O₂) measurements were performed on 2.0 mL aliquots of the siloxene aqueous solution that were withdrawn after varying periods of irradiation. For each test, a 0.5 mL volume of 1% *o*-tolidine in 0.1 M HCl was added to the suspension along with 1.0 mL of colloidal platinum as a catalyst, prepared as previously reported.⁵⁻⁶ This mixture was allowed to react for 2 min. A blue color indicative of oxidized *o*-tolidine formed within a very short time. Subsequently, the dispersion was acidified with 1M HCl (2 mL), producing a yellow color. The yellow species is the protonated form of the 2-electron oxidation product of *o*-tolidine formed. The resultant dispersions were then centrifuged at 12000 rpm for 2 min and the absorption spectrum of the supernatant (top four-fifth of the centrifuged dispersion) was immediately recorded with a UV-Vis spectrophotometer. The 2-electron oxidized *o*-tolidine product has an absorption maximum at 447 nm.

Concentration of Hydrogen peroxides determined by the calibrated curve and fitting equation: The calibrated curve and fitting equation was obtained using H₂O₂ with different concentration as external standard materials. The technique of *o*-tolidine as H₂O₂ indicator was in fact the quick oxidation reaction of *o*-tolidine and H₂O₂ catalyzed by colloidal Pt,⁵⁻⁶ forming a diimine which can be identified by its characteristic color. Without the Pt catalyst, the colorization reaction was slow. The testing process was similar to the mentioned in 2.

S2. Analysis of the hydrolysis process

The as-prepared siloxene achieved a small amount of hydrogen production from pure water in the dark (Figure 4a, curve (ii)). These results indicate that siloxene nanosheets can spontaneously react with water to produce hydrogen. To elucidate the reaction mechanism between siloxene with water, we have collected the hydrolysate and employed Fourier-transform infrared spectroscopy (FT-IR) to study the surface chemistry of both pristine siloxene nanosheets and hydrolysate, which is shown in Figure. S4. The assignments to the main absorption bands are given in Table 1. The pristine siloxene nanosheets feature band contain Si-H bonds, Si-Si bonds and Si-O-Si

bonds, corresponding to Si-H bending at 640 cm^{-1} , Si-H stretching at 2100 cm^{-1} , Si-Si stretching at about 520 cm^{-1} , Si-O-Si bending at 451 cm^{-1} and stretching at 1080 cm^{-1} respectively. After the hydrolysis reaction finished, the Si-H and Si-Si vibrational peaks vanished while both the peaks at 800 cm^{-1} responsible for Si-OH stretching and 940 cm^{-1} responsible for Si-O-Si stretching appeared. Besides, the intensity of peaks at 451 cm^{-1} and 1080 cm^{-1} responsible for Si-O-Si bending and stretching significantly increased. As a result, we believed the relevance of siloxene-water reaction to Si-H and Si-Si bonds. According to the results that we discussed above and referring relevant literatures^{1,7}, we proposed that the Si-H bonds and the Si-Si bonds of ($\text{Si}_6\text{H}_6\text{O}_3$) were oxidized to Si-OH bonds and Si-O-Si structure during the reaction, respectively, which are shown in the following equations:

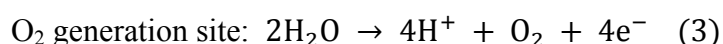
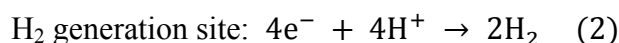
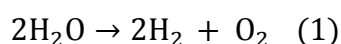


Based on these two equations, we can see the theoretical maximum amount of hydrogen generation can reach 40.54 mmol of hydrogen per g of initial siloxene nanosheets. In this work, 6.78 mmol g^{-1} of H_2 was produced in the first 6 hours and 27.88 mmol g^{-1} of H_2 during 60 hours. With the benefits of easy fabrication, low cost and earth-abundant, siloxene nanosheet also has the potential to act as a chemical hydrogen storage material.

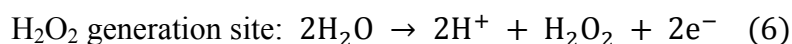
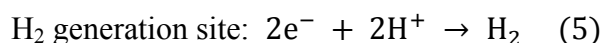
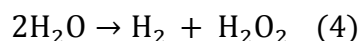
S3. Analysis of the water splitting process.

In a photocatalytic water splitting process the catalyst is excited with photos with energy higher than (or equal to) the bandgap, electrons and holes are separated. The electrons and holes migrate to the surface active sites, respectively.

The typical four-electron oxidation process for water splitting is:



While the two-electron water oxidation process is as follows:



The concerted four-electron process always requires large overpotential to overcome and induces kinetically competing two-electron reaction to H_2O_2 . Even though the four-electron water splitting process is thermodynamically more favorable than the two-electron oxidation path forming H_2O_2 , water splitting to H_2O_2 is kinetically favored with respect to the four-electron process. For this reason, water can be oxidized via a two-electron reaction to H_2O_2 and H_2 .

S4. Analysis of the degradation process of H_2O_2 that generated by photocatalytic water splitting

As is known, H_2O_2 molecules can be decomposed to hydroxyl radicals ($\cdot\text{OH}$) under Ultraviolet light irradiation, since the absorption edge of H_2O_2 is around 360 nm.⁸⁻⁹ Hence, a photoluminescence method with terephthalic acid (TA) as the probe molecule¹⁰ and Electron resonance (ESR) spectrum were employed to detect whether the $\cdot\text{OH}$ radicals were formed in the reaction system under light irradiation. As shown in Figure. S7, under simulated sunlight, TA captures $\cdot\text{OH}$ radicals to produce 2-hydroxyterephthalic acid (TAOH), which emits a unique fluorescence signal its peak centered at about 426 nm. The increasing fluorescence intensities clearly

confirm the form of $\cdot\text{OH}$ radicals in the process of light irradiation. As shown in Figure. S8, the siloxene aqueous solution after irradiation for 1 h under simulated sunlight shows a strong four-line ESR spectrum with relative intensities of 1:2:2:1, which is a characteristic of the DMPO- $\cdot\text{OH}$ spin adduct, while no ESR signal was observed in the blank experiment. For comparison, control experiment was performed under the same conditions in the presence of the H_2O_2 scavenging enzyme catalase¹¹. No signal can be detected when catalase was added to the reaction solution, suggesting that $\cdot\text{OH}$ radicals indeed originate from the reduction of H_2O_2 generated from water splitting. All these results clearly demonstrate that photogenerated H_2O_2 take place a degradation process during the photocatalytic water splitting.

S5. Additional characterization information

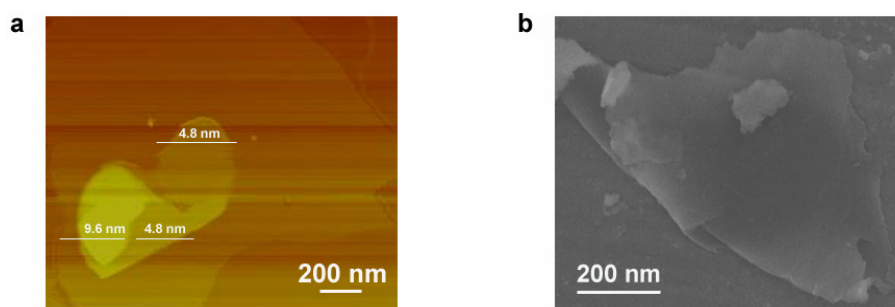


Figure S1. (a) AFM image and (b) SEM image of the obtained ultrathin siloxene nanosheets.

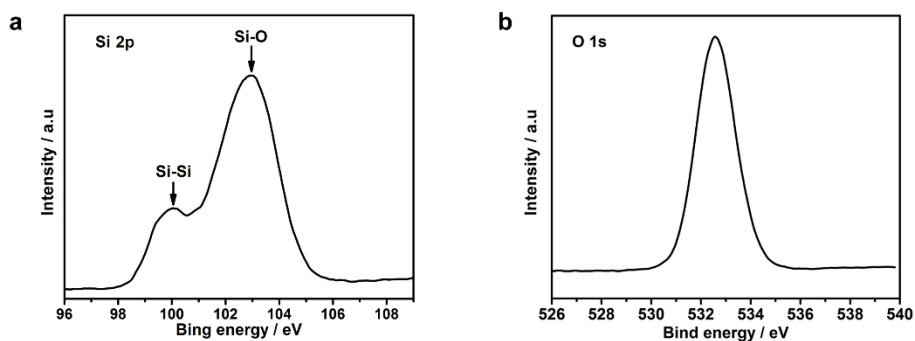


Figure S2. (a) Si 2p spectrum (b) O 1s spectrum of the siloxene nanosheets.

In the Si 2p spectrum, binding energy located at about 99.9 and 103.0 eV, corresponding to Si-Si bonds and Si-O bonds of the two-dimensional Si chain network, respectively. The 532.6 eV peak in the O 1s spectrum corresponds to the Si-O bonds.

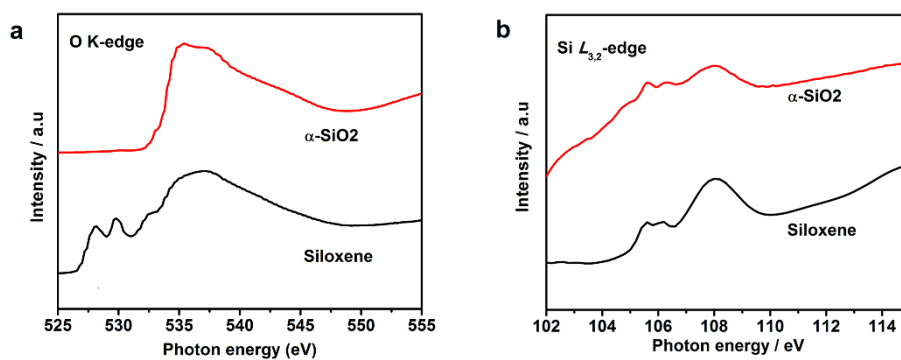


Figure S3. (a) The O *K*-edge and (b) Si *L*_{3,2}-edge XANES spectra.

The near-neighbor local structure of the siloxene was examined using X-ray absorption near edge structure (XANES) spectroscopy. The O *K*-edge and Si *L*_{3,2}-edge absorption spectra for as-prepared siloxene nanosheets are compared with the corresponding XANES spectra from the amorphous SiO₂. Of note, O *K*-edge XANES spectroscopy probes the unoccupied O 2p projected states, which could be hybridized with silicon states, while Si *L*_{3,2}-edge XANES spectroscopy involves the electron

transition of Si 2p states, and it is also sensitive to the oxidation state. As depicted in Figure S3a, the O *K*-edge spectrum from siloxene nanosheet presents new well-resolved peaks at ~ 530 eV, which could be due to its π -conjugated electronic structure, split into Si $3dt_{2g}$ and e_g states. In the Si $L_{3,2}$ -edge (Figure S3b) spectrum, the main features are similar to those observed from the α -SiO₂ thin film. A key difference is that the peak ratio of the first well-resolved peaks (around 106 eV). The first well-resolved peaks appear as a spin-orbit doublet associated with the transitions of Si 2p ($2p_{3/2}$ and $2p_{1/2}$) core states to the first unoccupied 3s-like states. It is generally agreed that relative peak ratio of the first two peaks relate to Si-O bonds and the peak ratio of first : second peak increases with the increase in shared oxygen atoms. Clearly, the peak ratio of first: second peak of siloxene is slightly smaller than that of α -SiO₂. This agrees well with the fact that more Si-O bonds exist in α -SiO₂. The XANES analysis further confirms the structural configuration of siloxene nanosheet is formed by an array of linear Si chains interconnected with oxygen bridges.

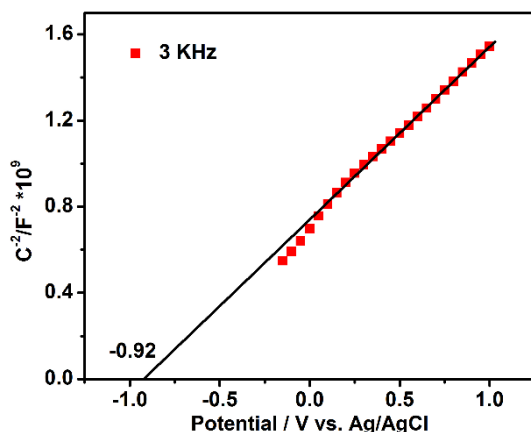


Figure S4. Mott-Schottky plot of siloxene nanosheets according to impedance measurement. The flat band potential was estimated from the intercept of the extrapolated line to be -0.92 V.

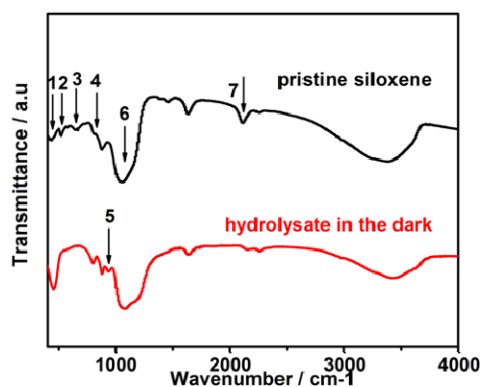


Table 1
Assignments of Some Characteristic
Absorption Bands of Siloxene

number	absorption (cm-1)	assignment
1	438-460	Si-O-Si bending
2	520	Si-Si stretching
3	640	Si-H bending
4	800	Si-OH stretching
5	940	Si-O-Si stretching
6	1040-1160	Si-O-Si stretching
7	2100	Si-H stretching

Figure S5. FT-IR spectra of the pristine siloxene and its hydrolysate in the dark.

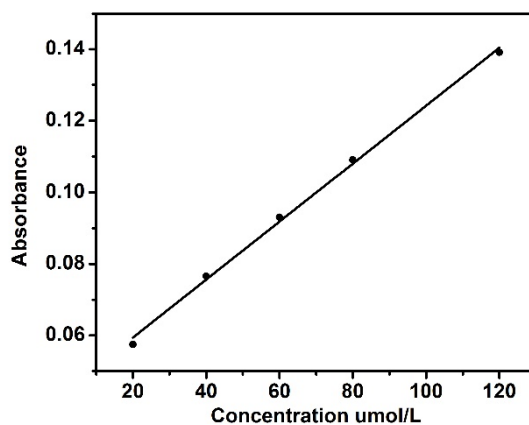


Figure S6. The calibration curve and the fitting equation of the H_2O_2 concentration and absorbance, which are determined by external standard method using H_2O_2 as standard materials with different concentration from 20 to 120 $\mu\text{mol/L}$ under the same experimental conditions.

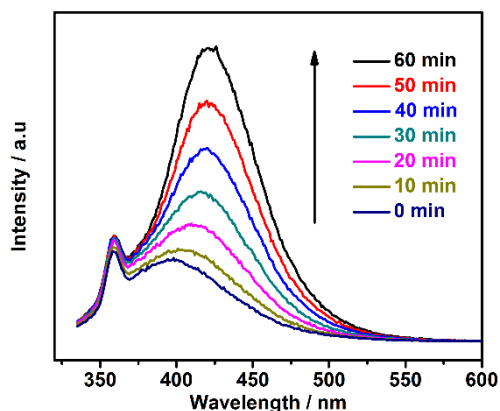


Figure S7. Time-dependent fluorescence emission spectra of TAOH formed by the reaction of TA with $\cdot\text{OH}$ radicals generated by siloxene nanosheets under simulated sunlight.

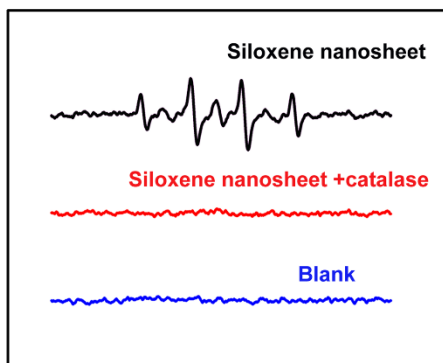


Figure S8. ESR spectra of siloxene nanosheets in the presence of DMPO in different conditions.

Reference:

1. A. Weiss, G. Beil and H. Meyer, *Z. Naturforsch.*, 1979, **35**, 25-30.
2. H. D. Fuchs, M. Stutzmann, M. S. Brandt, M. Rosenbauer, J. Weber, A. Breitschwerdt, P. Deak and M. Cardona, *Phys. Rev. B.*, 1993, **48**, 8172-8190.
3. J. R. Dahn, B. M. Way and E. Fuller, *Phys. Rev. B.*, 1993, **48**, 17872-17878.
4. S. Yanabaka, H. Matsu-ura and M. Ishikawa, *Mater. Res. Bulletin.*, 1996, **31**, 307-316.

5. D. Duonghong and M. Gratzel, *J. Chem. Soc., Chem. Commun.*, 1984, **1073**, 1597-1599.
6. J. Kimi and M. Graetzel, *J. Mol. Catal.*, 1987, 39, 63-70.
7. C. Zhan, P. K. Chu, D. Ren, Y. Xin, K. Huo, Y. Zou and N. K. Huang, *Int. J. Hydrogen Energy.*, 2011, **36**, 4513-4517.
8. J. L. Weeks and M. S. Matheson, *Trans. Faraday Soc.*, 1956, **78**, 1273-1278.
9. D. E. Lea, *Trans. Faraday Soc.*, 1949, **45**, 81-85.
10. G. Liu, L. Wang, C. Sun, X. Yan, X. Wang, Z. Chen, S. C. Smith, H.M. Cheng and G. Q. Lu, *Chem. Mater.*, 2009, **21**, 1266-1274.
11. T. Wu, T. Lin, J. Zhao, H. Hidaka and N. Serpone, *Environ. Sci. Technol.*, 1999, **33**, 1379-1387.